SLAC-PUB-2211
October, 1978
(Rev. Dec.,1978

Calculation of Neutron Yields Released by Electrons near the Photoneutron Threshold(*)

William P. Swanson
Stanford Linear Accelerator Center
Stanford, California 94305

December 12, 1978

ABSTRACT

Calculations are presented of yields of low-energy neutrons released by electrons incident on semi-infinite targets of natural C, Al, Fe, Ni, Cu, Ag, Ba, Ta, W, Au Pb and U. Yields are based on photon differential track-length distributions derived for semi-infinite targets from Approximation B of analytical shower theory. By the introduction of additional corrections in the treatment of the photon track-length distributions, calculational accuracy in the electron energy region near the photo-neutron threshold is considerably improved over a previous report. The calculations confirm the yields of the previous report for high incident electron energies but show them to be overestimates close to threshold. Systematics of yields are re-examined and a parameterization is offered which can be used to estimate yields very close to the threshold for any material. Results are relevant to the energy range used for radiation therapy.

(To be published in Health Physics)

(*) Work supported by the Department of Energy under Contract No. EY-76-C-03-0515.

INTRODUCTION

In a previous report (Sw78), a technique was described which was used to calculate the yield of low energy neutrons released when electrons are incident on targets of a variety of materials. It was found that, when referred to unit incident electron beam power, the yield from each material exhibited a sigmoid behavior, rising from threshold k_{th} to approach a nearly constant "saturation" value at high electron energies. The average trend of the saturation yield with atomic number was found to be approximately proportional to $Z^{0.73}$. This paper is an extension of the previous work and it considerably improves the accuracy of yields in the rapidly rising region close to the photoneutron threshold. The new calculations are therefore especially relevant to the energy range used for radiation therapy and also serve to confirm the previous results at high energy. For an extensive discussion of neutron production by electron beams and comprehensive references to earlier literature, the previous paper may be useful to the reader.

CALCULATION

As in Sw78, we assume that the entire electromagnetic cascade is totally absorbed in semi-infinite volumes of the chosen materials, but disregard attenuation of the resulting neutron fluences. The yield of neutrons (per incident electron) is given by the expression

$$Y(E_0) = \frac{N_0 \rho}{A} \int_{k_{th}}^{E_0} \sigma_n(k) \, \frac{dL^{\gamma}}{dk}(E_0, k) \, dk \ , \qquad (1)$$

(per electron)

where E_0 is the incident electron kinetic energy, N_0 is Avogadro's number, ρ is the material density, A the atomic weight, k the photon energy, dL^{γ}/dk the photon differential track length and $\sigma_n = \sigma(\gamma, n) + \sigma(\gamma, np) + 2\sigma(\gamma, 2n) + \cdots$ is the photoneutron yield cross section, which takes neutron multiplicity explicitly into account. The photoneutron threshold energy k_{th} lies in the range 6 - 13 MeV for most materials, and all of the photoneutron cross sections go through a peak due to a process generally known as the "giant resonance" (see, for example, Be75, Fu76). The cross sections used in the calculation are parameterizations of cross sections obtained with quasi-monoenergetic photons given in the compilation by Berman (Be76). Above 25 - 30 MeV, the cross sections of Jones and Terwilliger (Jo53) are used. See Table 1 of Sw78 for a complete list of original cross

section sources and all other material parameters.(*)

(*)The following minor modifications are made in the data of this table:

a) The cross sections for ^{206}Pb and ^{207}Pb of Ha64 are multiplied by 1.36, obtained from the ratio $\sigma_m\Gamma$(Ve70) / $\sigma_m\Gamma$(Ha64), where σ_m and Γ are the peak cross section and resonance width for ^{208}Pb, respectively, as given in Table I of Be76. This scaling was suggested by E. G. Fuller (Fu78) and, when used together with cross sections of Ve70 for ^{208}Pb, results in a consistent normalization for the three main isotopes of natural Pb.

b) The effective photofission threshold for U is lowered to 5.4 MeV (see, for example, Di75), and the (γ, n) threshold is corrected to 6.13 MeV.

The photon differential track length appearing in equation (1) is obtained by an integration of the electron differential track length dL^e/dE from the photon energy in question k to the maximum electron energy of the shower

$$\frac{dL^\gamma}{dk}(E_0, k) = F^\gamma(k) \frac{X_p}{X_0} \frac{N_0 \rho X_0}{A} \int_k^{E_0} \frac{d\sigma^B}{dk}(E, k) \frac{dL^e}{dE}(E_0, E)\, dE , \qquad (2)$$

where X_0 is the radiation length (values are from Tsai (Ts74)), ($F^\gamma X_p$) is the average distance traveled by a photon of energy k before interaction and $d\sigma^B/dk$ is

the bremsstrahlung cross section (per atom), differential in k. The factor $F^{\gamma}(k)$ is a variable in the approximate range 1 - 3 (see Fig. 2 of Sw78) and, at high k, X_p is approximately equal to (9/7) X_0. Comparison of equation (2) with equation (3) of Sw78 reveals the difference to be the replacement of

$$X_0 \frac{dN^{\gamma}}{dX}(E, k) = F^{e}(E) \; / \; k \qquad \text{by} \qquad (3a)$$

$$X_0 \frac{dN^{\gamma}}{dX}(E, k) = \frac{N_0 \rho X_0}{A} \cdot \frac{d\sigma^{B}}{dk}(E, k) \; ; \qquad (3b)$$

i.e., by the replacement of a "rectangular" bremsstrahlung spectrum by a "natural" spectrum of the same total energy radiated per unit of electron path.(*) This is the more

---

(*) Over the largest range of E and k that occur, $d\sigma^{B}/dk(E, k)$ is calculated using equations 3CS (for $\gamma < 2$) and 3CS(d) (for $2 < \gamma < 15$), where the equation numbers are those of Koch and Motz (Ko59). (Note that E of this report signifies kinetic energy. This is transformed to total energy E_{tot} for use in the cited formulae.) The parameter γ is the screening parameter $\gamma = 100\, k\, m_e / E_{tot}(E_{tot} - k)\, Z^{1/3}$, where $E_{tot} = E + m_e$ and m_e is the electronic mass 0.511 MeV. For E < 15 MeV, $f(Z)$ is set equal to zero in both equations, reducing them to equations 3BS and 3BS(d), respectively; otherwise $f(Z)$ is as given on p. 928 of Ko59.

For $\gamma > 15$, equation 3BN is used at all E instead. This alternative form applies only for k very close to E. A minimum bremsstrahlung cross section is also imposed, interpolated from Fig. 12 of Ko59.

---

important of the two modifications made in this utilization of Approximation B as compared to the calculation described in Sw78.

The electron differential track length dL^e/dk which underlies the calculation of the photon track length for equation (2) is given by:

$$\frac{dL^e}{dE}(E_0, E) = \frac{F^e(E_0)\ E_0\ X_0}{0.437\ \epsilon_0^2} \left[\frac{1}{x} - (1 + x)\, e^x \int_x^{x_0} \frac{e^{-s}}{s^2}\, ds\right] , \qquad (4)$$

where ϵ_0 is the energy loss by ionization per electron per radiation length X_0 and is therefore approximately equal to the "critical energy". Actual values of this parameter (see Table 1) are computed from $dE/dX\big|_{col}$ at E = 30 MeV, as tabulated by Berger and Seltzer (Be64). Apart from the extra factor $F^e(E_0)$ and the definitions of x and x_0, equation (4) is the same as proposed by Tamm and Belenky (Ta39; also see Ro41, Ro52). In the Tamm-Belenky formulation, x and x_0 represent the reduced energies $x = E/0.437\ \epsilon_0$ and $x_0 = E_0/0.437\ \epsilon_0$, respectively. However, for this calculation, these are replaced by

$$x = F^e(E_0)\ E\ /\ 0.437\ \epsilon_0 \qquad \text{and} \qquad (5a)$$

$$x_0 = F^e(E_0)\ E_0\ /\ 0.437\ \epsilon_0\ . \qquad (5b)$$

$F^e(E_0)$ is the ratio of the electron's fractional energy loss by bremsstrahlung per unit path length at energy E_0 to that at infinite energy, and varies in the approximate range 0.7 - 0.9 for the materials and energies considered here (see Fig. 1 of Sw78). These variables express the relationship of bremsstrahlung energy loss to ionization loss (this ratio is nominally E/ϵ_0), and this modification tends to correct this relationship in the energy range considered. The relative shape of the electron track length distribution is purely a function of x and x_0 (in the bracketed term of equation (4)) and this substitution should improve the relative shape, particularly near the tip ($E \approx E_0$), which contributes greatly to the photon differential track length distribution at low E_0. In addition, the coefficient of equation (4) contains the extra factor $F^e(E_0)$. The resulting distributions, while improved in relative shape, especially for lower E_0/ϵ_0, retain the correct limiting behavior: They show a rise near $E = E_0$ to a value $dL^e/dX = X_0/\epsilon_0$, and the integral track length $L^e \equiv \int dL^e/dE\ dE$ is equal to $X_0\ E_0/\epsilon_0$, as is required by conservation of energy for constant $dE/dX\big|_{col} = \epsilon_0/X_0$. The limit of very large ϵ_0/E_0 gives a

constant electron distribution equal to X_0/ϵ_0 and a small ϵ_0/E_0 causes the distribution to approach Approximation A, independent of ϵ_0. (See discussion of these points on p. 357 of Sw78.) This transformation in the x-variables is the second modification made, as compared to the calculation of Sw78. Because it enhances the upper part of the electron spectrum somewhat (at the expense of the lower part), it results in photon differential track lengths larger by 0 - 10%, while not strongly affecting their relative shape. The effect on the neutron yields is to raise them by about 5 - 10%.

The resulting photon differential track length distributions are shown in Figs. 1 - 4 for Pb, Cu, Al and C. They differ from the corresponding figures of Sw78 mainly in that the final slopes are less steep. This is because the "natural" bremsstrahlung spectra "slump" towards higher k, particularly at low primary electron energies, rather than being perfectly "rectangular" as was implicitly assumed in Sw78 (equation (3b) vs. (3a)). In the uncorrected Approximation B which uses "rectangular" bremsstrahlung spectra (equation (3a)), the initial rise ($k \approx 0$) and final decline ($k \approx E_0$) of each curve are tangent to lines with slopes of magnitude $(9/7)(1/\epsilon_0)$. Such lines are labeled "S" to the right and left of Figs. 1 - 4. The importance of using the "natural" bremsstrahlung spectra (equation (3b)) is best appreciated by noting the departure of the calculated curves from these lines (cf. Figs. 6 and 7 of Sw78).

NEUTRON YIELDS

Yields resulting from evaluation of equations (1, 2 and 4) by numerical integration are shown in Figs. 5 and 6. The main qualitative difference from the corresponding results of Sw78 (Figs. 8, 9 of Sw78) is the more gradual approach to "saturation", i.e., a smaller slope on the rising portions. This is a result of the slower falloff of the photon distributions evident in Figs. 1 - 4, which in turn is a consequence of the "natural" bremsstrahlung shape, introduced via equation (3b). Qualitatively, the midpoints of the rising curves of Fig. 5 are shifted (relative to Sw78) by about 4 MeV for medium and heavy nuclei and somewhat more than this for low Z (about 5 and 7 MeV for Al and C, respectively). The "shoulders", which occur at roughly twice the giant resonance peak energy, are shifted by about the same amounts. The shoulders are less pronounced than for the corresponding calculations of Sw78, and the yields continue to rise in the region of the high-energy "plateaux". However, the high-energy yields are not significantly different in the new calculation; the new values are changed by an average of only +3% at E_0 = 100 MeV (Fig. 6). (Lead (Pb) is higher by 13.5% at 100 MeV mainly because of the larger cross sections used in this calculation; see footnote, p. 4.) Table 1 shows calculated yields at discrete energies. In order to present a consistent set for this publication, recomputed values for

E_0 = 100, 150, 500 and 1000 MeV are also given. In computing yields at 500 and 1000 MeV, the integration is extended only to k = 150 MeV, as was also done in Sw78(*)

(*) We take this opportunity to correct a minor mistake in a footnote concerning the cut in integration on p. 359 of Sw78. For infinite incident energy E_0, the amount of neutrons produced by photons above 150 MeV is about 4% for most nuclei but rises at low Z to about 12 and 16% for Al and C, respectively. This is more than the 1% claimed in the original footnote for medium-weight nuclei. Nevertheless the cut in integration is made at k = 150 MeV, with no correction for higher photon energies, as it is the number of low-energy neutrons that is being calculated, and not those involving photopion processes which occur at k > 140 MeV.

Because the slopes of the curves of Fig. 5 are significantly changed, the ratios of these yields to those given by Approximation A (Ro41, Ro52; see equation (4) of Sw78) are considerably affected at lower E_0. Figure 11 of Sw78 has been modified accordingly and is given here as Fig. 7. The curves for E_0 = 50 MeV and higher look almost the same as before whereas those for E_0 = 10, 15 MeV are lowered by about a factor of two by the new calculations.

Although the change is not very significant, the high-

energy values are somewhat shifted, and therefore the overall trend with atomic number is also altered. The parameters of equation (5) of Sw78 have been redetermined using the new yields at E_0 = 500 - 1000 MeV. The revised expression is

$$Y(\text{neutrons sec}^{-1}\ \text{kW}^{-1}) = (1.34 \pm 0.16)\cdot 10^{12}\ (Z/37.5)^{(0.66 \pm 0.05)} = 1.21\cdot 10^{11}\ Z^{(0.66 \pm 0.05)} \quad (6)$$

As before, ten materials are used for the fit, with Ni and U excluded as "atypical". The yields for low Z (C - Cu) have increased somewhat at 500 and 1000 MeV, but there is a slight decrease at high Z, relative to Sw78 (apart from Pb, for which a different cross section is used). Yields for Ag and Ba are almost unchanged. These adjustments manifest themselves as a lessening of the Z dependence (i.e., the exponent is 0.66 ± 0.05 instead of 0.73 ± 0.05). However, there is no significant change in the coefficient of equation (6), which means that the average saturation yield is not much affected by the modified calculation. (Comparing the first form of the equation, we now have 1.34 ± 0.16 instead of 1.3 ± 0.2 from Sw78; the first form has the advantage that the errors in the parameters are uncorrelated, i.e., the off-diagonal elements of the covariance matrix are zero.) The errors quoted in equation (6) reflect only the variance of data about the fitted curve

and do not explicitly include the calculational uncertainty discussed below. Although the difference is not very significant, the version of equation (6) given here is preferred to that of Sw78 because it is consistent with the yields calculated for low E_0, and it also reflects the modification in the Pb cross sections (see footnote, p. 4).

The uncertainty in the yields can be regarded as arising from two sources: biases in the photon differential track length distributions and errors in the elementary cross section measurements (cf. equation (1)). The accuracy of the photon distributions can best be estimated by comparison with the same distributions calculated by Monte-Carlo methods. Comparison with published Monte-Carlo distributions (Al66, Ga69, Ze62) suggests that they are probably correct to ±10% for Cu and Pb in the region of the giant-resonance peak for $E_0 \lesssim 50$ MeV (see examples in Figs. 1 and 2). The same type of comparison with unpublished track length distributions calculated at SLAC (Fo78, Ma78) has confirmed that, for Al, Cu and Pb, the track length distributions in the region of the giant resonance are given correctly to ±7% over the range E_0 = 0 - 50 MeV, but the distribution for C tends to be too low by about 10 - 12%. At higher energies (E_0 = 100, 500 MeV), there is a tendency to underestimate the photon distribution by about 14% for C, 9% for Al, and by 5% for Cu - Pb in the region of the giant resonance peak. This underestimation may be due to the "buildup" of Compton-scattered photons, analogous to the

effect observed in ordinary radiation shielding; buildup of this sort is not taken into account. Considering also theoretical uncertainties, we believe that the error in neutron yield arising solely from the photon distributions given by equations (2) - (4) is ±13% for C and ±8% for Al - U, for $E_0 \lesssim 50$ MeV. For $E_0 > 50$ MeV, the errors are believed to be about ±16% for C, ±12% for Al and ±9% for Fe - U.

The overall uncertainty in neutron yield must also reflect errors in the elementary cross section measurements. If these are taken to be ±15% (Fu78) in the region of the giant-resonance peak and combined in quadrature with the errors of the preceding paragraph, the overall error in neutron yield is less than ±20% for all materials (but ±22% for C), at all E_0 except within about 6 - 8 MeV of threshold. Here, accuracy is vitiated by the lack of near-threshold cross-section data. This is discussed in the following section. (The overall accuracy claimed for the previous calculation (Sw78) was ±20% of the saturation values.)

YIELDS VERY CLOSE TO THRESHOLD

Insofar as they are available, measurements of photoneutron cross sections with quasi-monoenergetic photons very close to threshold have larger relative errors, and any simple parameterization is likely to obscure considerable structure. Nevertheless yield calculations based on simple parameterizations are undoubtedly useful if their approximate nature is realized by the user. The primary parameterization chosen is a straight line rising from zero at k_{th} to join smoothly onto the available cross section measurements at about $E_0 - k_{th} = 2$ MeV. As it is not certain that this is an accurate portrayal of the actual cross section behavior, the resulting yields must be used with some caution at energies within a few MeV of threshold. Within this energy region the error in the yield might be as large as a factor of two with this parameterization. (As the accuracy in the photon track length distributions is quite good at lower energies (±13% for C, ±8% for Al - U), practically all of this error is from the cross sections.) However, as $E_0 - k_{th}$ is increased, the relative error decreases; for $E_0 - k_{th} = 6 - 8$ MeV, uncertainties due to the near-threshold cross sections are only about ±10%, and become less at higher E_0, in inverse proportion to the yield. The "saturation" values are affected only by about 1 - 2% by uncertainties in the near-threshold cross sections.

Table 2 shows values of initial cross section slopes

assumed (left-hand portion). These values should not be taken too literally as they are only hand-interpolations drawn without theoretical guidance; the hypothesis of a linear cross section near k_{th} is only an assumption, albeit a perfectly reasonable one.

Figure 8(a) shows the resulting yields, plotted as functions of $(E_0 - k_{th})$. Most of the plotted yields are based on a single parameterization for the natural material and show a smooth, almost log-linear behavior over most of the range shown. On the other hand, Ni, Cu and Pb are based on parameterizations for the separate contributing isotopes, which are explicitly combined to give the total, with $(E_0 - k_{th})$ measured from the lowest threshold. Each separate contribution manifests itself as a change in slope, most pronounced for Pb, where three isotopes contribute significantly. Similarly, the curve for U shows an inflection caused by differing thresholds for the photofission and photoneutron effects.

The curves of Fig. 8(a) can be approximated at low energy by a power law in which the yield is proportional to $(E_0 - k_{th})^N$, where the exponent N is about 3. That the exponent N is close to 3 can be explained as follows: The yield is the convolution of two functions of k, one of which is assumed to rise exactly linearly from zero at k_{th} (the cross section) and the other can be assumed to decline linearly to zero at E_0 over the limited range considered

(the photon differential track length distribution near the tip). Such a convolution yields a single term proportional to the cube of the difference in integration limits: $(E_0 - k_{th})^3$.

As the yields are directly proportional to the cross-section slopes assumed, the user of these data can scale these results by another slope-value as better measurements become available. The results can also be readily adapted to other materials of similar Z by such scaling.

Using a rough approximation for the photon spectrum, namely the "rectangular" bremsstrahlung spectrum of equation (3a), we estimate the yield per electron $Y(E_0 - k_{th})$ to be on the order of

$$Y(E_0 - k_{th}) \simeq \left\{\frac{9}{7} F^e(k_{th}) \; F^\gamma(k_{th})\right\} \cdot \left[\frac{N_0 \rho X_0 S}{6 A \epsilon_0 k_{th}}\right] (E_0 - k_{th})^3$$

(order of magnitude, per electron) (7)

where S is the slope (cm^2/MeV) of the assumed linear cross sectional rise, and the other factors are defined in connection with equations (1) - (4). Apart from the factors F^e and F^γ, equation (7) is derived from a photon distribution given by a straight line (in the units of Figs. 1 - 4) of slope $-(9/7)(1/\epsilon_0)$ which intercepts the k-axis at $k = E_0$. This is illustrated by lines labeled "S" in Figs. 1 - 4 for E_0 = 35 MeV and these clearly give overestimates for all materials. Although meant only as a very rough approximation,

equation (7) is instructive in showing sources of the most important material-dependent factors. The first group of factors (within braces) is on the order of (but greater than) unity for all materials and the main material dependence is contained in the second factor (bracketed). The strongest energy dependence is contained in the term $(E_0 - k_{th})^3$. Figure 9(a) and Table 2 show empirical values of the "reduced yield", i.e., the yield at $E_0 - k_{th} = 1.0$ MeV divided by the second factor of equation (7)

$$Y_R(\text{lin}) \equiv Y(1.0) \Big/ \left[\frac{N_0 \rho X_0 S}{6 A \epsilon_0 k_{th}}\right] , \qquad (8)$$

as a function of the atomic number Z.(*) Also given in Fig.

(*) The near-threshold parameters of Fig. 9 and Table 2 are given in terms of neutrons per electron because showering does not play an important role in producing yields at small $(E_0 - k_{th})$, i.e., the photons which excite photoneutron events are almost all radiated by the "original", rather than progeny, electrons. (On the other hand, the data of Figs. 5, 6, 8 and Table 1 are normalized to incident beam power because such a presentation demonstrates the convenient scaling with power when showering does play a dominant role at higher E_0.) The conversion of units is simply: $(1.602\ 10^{-16}\ E_0)$ Y(neutrons $\text{sec}^{-1}\ \text{kW}^{-1}$) = Y(neutrons/electron), where E_0 is in MeV.

---

9 and Table 2 are empirical values of N(lin), averaged over intervals in $(E_0 - k_{th})$ near 1.0 MeV. These correspond to and replace the exponent 3 of equation (7). To avoid the complication of multiple thresholds for Ni, Cu and Pb (apparent in Fig. 8), the points of Fig. 9 are only for the pure isotopes (specifically: ^{60}Ni, average of ^{63}Cu and ^{65}Cu, and, separately, ^{206}Pb, ^{207}Pb and ^{208}Pb). The regularity of these empirical parameters with Z is readily apparent in this figure, where each datum corresponds to a unique threshold and related cross section slope. Values of $Y_R(lin)$ are all less than unity and rise linearly with Z. Deviation from unity is approximately proportional to the factor by which the straight lines of slope $-(9/7)(1/\epsilon_0)$ of Figs. 1 - 4 fail to describe the photon differential track lengths at $k \approx E_0$. Evidently, the larger Z is, the better equation (7) describes the neutron yield. That is, $Y_R(lin)$ is closest to unity and N(lin) closest to 3 for largest k_{th}/ϵ_0. Values of $Y_R(lin)$ and N(lin) can be easily interpolated from Fig. 9, and the neutron yield per electron near threshold estimated for any target nuclide by

$$Y(E_0 - k_{th}) = Y_R\,(E_0 - k_{th})^N, \qquad (9)$$
$$\text{(per electron)}$$

where E_0 and k_{th} are in MeV. Where more than one target isotope is involved, they may be calculated separately and

then combined, with each component weighted by its fractional amount in the material in question.

Although a near-threshold yield is calculated for U for Figs. 8, 9 and Table 2, it must be remembered that there is actually no well-defined threshold for neutron emission from U. Photofission can be excited by photons of any energy, although the cross section is much smaller than the (γ, n) cross section (above the (γ, n) threshold of 6.13 MeV) and is practically zero below about 5.4 MeV (Di75). For simplicity, parameters are derived for Fig. 9 and Table 2 using a nominal threshold of 6.00 MeV for both processes.

For comparison, an alternative formulation is used in which the photoneutron cross section $\sigma_n(k)$ is assumed to be given by a Lorentz resonance curve in the near-threshold energy range of Fig. 8:

$$\sigma_n(k) = \frac{\sigma_m}{1 + \left[(k^2 - k_m^2)^2 / k^2 \Gamma^2\right]} \qquad (10)$$

where σ_m is the maximum cross section, k_m is the photon energy at which the maximum occurs, and Γ the resonance width. Where appropriate, two such terms are combined. Resonance parameters are from Table I of Be76 and the resulting yields are shown in Fig. 8(b). Because in this parameterization the cross section is slowly varying and non-zero at k_{th}, the yields also vary more slowly; the

logarithmic slope is closer to N = 2, rather than 3, and yields are probably overestimated by a large factor at small $(E_0 - k_{th})$ although they are still very small compared to the "saturation" yields.

Analogous to equation (8), a reduced yield can be defined in terms of the threshold cross section $\sigma_n(k_{th})$, which in this formulation is nearly constant close to k_{th}:

$$Y_R(res) \equiv Y(1.0) \Big/ \left[\frac{N_0 \rho X_0 \sigma_n(k_{th})}{2 A \epsilon_0 k_{th}}\right]. \qquad (11)$$

Values of the parameters $Y_R(res)$, determined at $E_0 - k_{th} = 1.0$ MeV, and N(res), averaged over intervals in $(E_0 - k_{th})$ near 1.0 MeV are given in Table 2 and Fig. 9, for those of the 12 chosen materials for which resonance parameters are available. From the figure it appears that the exponent N(res) is less than N(lin) by about 0.7 - 0.9 and $Y_R(res)$ is comparable to, but somewhat greater than $Y_R(lin)$. Lighter elements (C, Al) are not well described by the resonance formula and are not included. Using the Lorentz resonance parameters as the basis of the photoneutron cross section places an absolute maximum on the neutron yield near threshold, because the resonance formula represents the sum of all dipole photonuclear reactions, and not all of these lead to neutron emission this close to threshold.

It should be noted that the beam from a real electron

accelerator may contain an energy spectrum of significant width. Where the neutron yield varies rapidly with each increment in E_0, as in Fig. 8, a reasonable estimate of the neutron yield can only be obtained by an integration over the electron spectrum. The type of parameterization presented here (equation (9), Table 2, Fig. 9) is convenient for this purpose.

SUMMARY AND CONCLUSIONS

As compared to the previous publication Sw78, two significant modifications are made in the method of using Approximation B to calculate neutron yields for low incident electron energies. Firstly, the "natural" bremsstrahlung spectrum has been substituted for the "rectangular" shape (equations (3)). Secondly, the reduced energies x and x_0 have been scaled to take better into account the actual relationship of electron energy loss by bremsstrahlung and by ionization (equations (5)).

While the results presented here are relatively more accurate in the rapidly-rising portions of Figs. 5 and 6, they have resulted in relatively little change in the yields above the "shoulders" of the curves. In general, they have shown the results of Sw78 to be overestimates in the region of the rise for each material while confirming those at "saturation". The conclusions of Sw78, particularly those of the section "Significance for Radiation Protection" are fully confirmed by the improved results.

It is worth noting that, in the energy range used for radiation therapy, the values for neutron yields given in the present work lie below those of the previous publication by as much as 50% at energies where they may represent a significant stray radiation field ($E_0 \gtrsim 15$ MeV), and have an uncertainty of less than about ±20%. In studies of risk to patients from neutron leakage, source terms based on the present calculations are preferred.

There is probably little to be gained at this time in further refinement of this calculational program. The accuracy of the photon differential track length distribution at all energies is comparable to, or better than that of the cross section measurements on which these yields are based, and a more accurate track length for thick targets would not result in a commensurate improvement in overall accuracy in yields. The results are sufficiently accurate as source terms for radiation-protection purposes. In practice, such perturbations on the neutron field as are due to inherent anisotropy, target thickness and shape, moderation and reflection by walls, and shielding by equipment will exceed the uncertainties in these calculated yields. If more accurate results are desired, especially for the treatment of particular geometries, Monte-Carlo methods are recommended both for the calculation of the photonuclear source term and neutron propagation within the radiation enclosure.

Helpful discussions with R. C. McCall and E. G. Fuller are gratefully acknowledged.

REFERENCES

Al66 Alsmiller R. G., Jr. and Moran H. S., 1966, Electron-Photon Cascade Calculations and Neutron Yields from Electrons in Thick Targets, Oak Ridge National Laboratory, Report No. ORNL-TM-1502; also see, 1967, Nucl. Instrum. Methods 48, 109.

Be64 Berger M. J. and Seltzer S. M., 1964, Tables of Energy Losses and Ranges of Electrons and Positrons, National Aeronautics and Space Administration, Report No. NASA SP-3012, Washington, D. C.

Be75 Berman B. L. and Fultz S. C., 1975, "Measurements of the Giant Dipole Resonance with Monoenergetic Photons", Rev. Mod. Phys. 47, 713.

Be76 Berman B. L., 1976, Atlas of Photoneutron Cross Sections Obtained with Monoenergetic Photons, Bicentennial Edition, Lawrence Livermore Laboratory, Report No. UCRL-78482. Also see 1975, "Atlas of Photoneutron Cross Sections Obtained with Monoenergetic Photons", Atomic Data Nucl. Data Tables 15, 319.

Di75 Dickey P. A. and Axel P., 1975, "^{238}U and ^{232}Th Photofission and Photoneutron Emission near Threshold", Phys. Rev. Lett. 35, 501.

Fo78 Ford R. L. and Nelson W. R., 1978, The EGS Code System: Computer Programs for the Monte Carlo Simulation of Electromagnetic Cascade Showers (Version 3), Stanford Linear Accelerator Center, Report No. SLAC-210, Stanford, CA.

Fu76 Fuller E. G. and Hayward E., 1976, Photonuclear Reactions (Stroudsburg, PA.: Dowden, Hutchinson and Ross).

Fu78 Fuller E. G., 1978, Private communication, National Bureau of Standards, Washington, D. C.

Ga69 Gabriel T. A. and Alsmiller R. G., Jr., 1969, Photonucleon and Photopion Production from High-Energy (50 to 400 MeV) Electrons in Thick Copper Targets, Oak Ridge National Laboratory, Report No. ORNL-4443, Oak Ridge, TN.

Ha64 Harvey R. R., Caldwell J. T., Bramblett R. L. and Fultz S. C., 1964, "Photoneutron Cross Sections of Pb^{206}, Pb^{207}, Pb^{208} and Bi^{209}", Phys. Rev. 136, B126.

Jo53 Jones L. W. and Terwilliger K. M., 1953, "Photoneutron Production Excitation Functions to 320 MeV", Phys. Rev. 91, 699.

Ko59 Koch H. W. and Motz J. W., 1959, "Bremsstrahlung Cross-Section Formulas and Related Data", Rev. Mod. Phys. 31, 920.

Ma78 Mark D. R. and Nelson W. R., 1978, Private communication, Stanford Linear Accelerator Center, Stanford, CA.

Ro41 Rossi B. and Greisen K., 1941, "Cosmic Ray Theory", Rev. Mod. Phys. 13, 240.

Ro52 Rossi B., 1952, High-Energy Particles, Chapter 5 (Englewood Cliffs, N. J.: Prentice-Hall).

Sw78 Swanson W. P., 1978, "Calculation of Neutron Yields Released by Electrons Incident on Selected Materials", Stanford Linear Accelerator Center, Report No. SLAC-PUB-2042, Rev.; and 1978, Health Phys. 35, 353.

Ta39 Tamm Ig. and Belenky S., 1939, "On the Soft Component of Cosmic Rays at Sea Level", J. Phys. (U.S.S.R.) I, 177.

Ts74 Tsai Y.-S., 1974, "Pair Production and Bremsstrahlung of Charged Leptons", Rev. Mod. Phys. 46, 828.

Ve70 Veyssière A., Beil H., Bergère R., Carlos P. and Leprêtre A., 1970, "Photoneutron Cross Sections of ^{208}Pb and ^{197}Au", Nucl. Phys. A159, 561.

Ze62 Zerby C. D. and Moran H. S., 1962, Studies of the Longitudinal Development of High-Energy Electron-Photon Cascade Showers in Copper, Oak Ridge National Laboratory, Report No. ORNL-3329, Oak Ridge, TN; see also 1963, "Studies of the Longitudinal Development of Electron-Photon Cascade Showers", J. Appl. Phys. 34, 2445.

FIGURE CAPTIONS

Fig. 1. Photon differential track length for Pb for incident electron kinetic energies in the range E_0 = 5 - 35 and 100 MeV. The dimensionless units $(k^2/X_0E_0)\ dL^\gamma/dk$ are used for easy comparison of different materials and energies. The Approximation A prediction is indicated at 0.572 for comparison. Straight lines S to left and right of graph have slopes of $+(9/7)(1/\epsilon_0)$ and $-(9/7)(1/\epsilon_0)$, respectively. The photoneutron cross section (barns), containing the neutron multiplicity, is also drawn, smoothed, to show relationship to the photon distributions. Threshold is indicated as k_{th}. Also shown is a Monte-Carlo calculation for 34-MeV electrons (10 X_0 Pb) from Alsmiller and Moran (Al66).

Fig. 2. As for Fig. 1 but for Cu. Note that ordinate scale changes for this figure as well as Figs. 3 and 4. The Monte-Carlo calculation is for 5 X_0 Cu at E_0 = 34 MeV (Al66). (The distribution near the cross section maximum for this target thickness is expected to be about 15% below that for a semi-infinite target.)

Fig. 3. As for Figs. 1 and 2 but for Al.

Fig. 4. As for Figs. 1 - 3 but for C.

Fig. 5. Neutron yields from semi-infinite targets of twelve natural materials per unit incident electron beam power, plotted as functions of incident electron kinetic energy E_0. Threshold for each material is indicated as a closed circle. Parameterization of cross section within 2 MeV of each threshold assumes a linear rise from zero at k_{th}. Accuracy is on the order of ±20% except for portions within 6 - 8 MeV of threshold (see text).

Fig. 6. As for Fig. 5, but extended to E_0 = 100 MeV.

Fig. 7. Ratio of neutron yield from semi-infinite targets according to the calculation described, to the yield predicted by Approximation A (equation (4) of Sw78), plotted as a function of target atomic number Z. Curves are interpolations of calculated points and parameter affixed to each curve is the incident electron energy E_0. There is no reason to expect a significant change at energies above 500 MeV. Apparent crossover for high Z at high E_0 is not regarded as significant.

Fig. 8. Neutron yields from semi-infinite targets of natural materials per unit incident electron beam power, plotted as functions of increment in incident electron kinetic energy over the photoneutron threshold ($E_0 - k_{th}$). Curves for Ni, Cu and Pb contain explicit contributions of isotopes having different thresholds. For U, both photoneutron and photofission processes are included, but with a common effective threshold arbitrarily set at 6.00 MeV. All other curves are based directly on cross sections measured for natural materials and only one threshold is assumed (see Table 2 for values).

(a) The (γ, n) cross section is assumed to rise linearly from zero at each threshold to join smoothly onto measurements at about $E_0 - k_{th} = 2$ MeV. This formulation is believed to give the more realistic yields as compared to the alternative form using Lorentz resonance parameterization for the cross sections.

(b) As for (a), except cross section near threshold is given by Lorentz resonance parameterization. This formulation gives a large overestimate near threshold and is mainly presented for comparison and to show an upper limit to neutron production. Relative differences between these yields and those of (a) diminish appreciably at higher E_0. This parameterization is not suitable for all materials.

Fig. 9. Empirical parameters describing neutron yields from semi-infinite targets within a few MeV of photoneutron threshold, plotted as functions of target atomic number Z. Underlying cross sections are assumed to rise linearly from threshold (lin) or, alternatively, to be given by the Lorentz resonance shape (res). Corresponding parameters are defined by equations (8) and (11), respectively. Solid curves are interpolations which may be used to estimate near-threshold neutron yield (per electron) for any material, by means of equation (9).

(a) Reduced yields Y_R(lin) and Y_R(res) are determined from yields calculated at $E_0 - k_{th} = 1.0$ MeV.

(b) Exponents N(lin) and N(res) are averaged over the intervals indicated: $(E_0 - k_{th}) = 0.1 - 1.0$, 0.5 - 2.0 and 1.0 - 2.0 MeV.

Table 1. Neutron yields for semi-infinite targets at selected incident electron kinetic energies E_0.

Natural Material	k_{th}[a] (MeV)	ϵ_0[b] (MeV)	Neutron Yield per Incident Electron Beam Power (neutrons sec^{-1} kW^{-1})[c]									
			10 MeV	15 MeV	20 MeV	25 MeV	34 MeV	50 MeV	100 MeV	150 MeV	500 MeV	1000 MeV
6 C	18.72	79.38	---	---	1.96(7)	8.15(9)	6.19(10)	1.56(11)	3.19(11)	3.86(11)	4.37(11)	4.40(11)
13 Al	13.03	41.95	---	4.59(7)	8.52(9)	5.07(10)	1.61(11)	3.13(11)	5.14(11)	5.80(11)	6.17(11)	6.20(11)
26 Fe	11.21	22.31	---	1.13(10)	9.65(10)	2.42(11)	4.31(11)	6.02(11)	7.62(11)	8.00(11)	8.17(11)	8.18(11)
28 Ni	11.38	21.00	---	3.89(9)	5.87(10)	1.57(11)	3.09(11)	4.77(11)	6.50(11)	7.07(11)	7.34(11)	7.36(11)
29 Cu	9.91	20.23	---	2.00(10)	1.56(11)	3.54(11)	6.35(11)	8.76(11)	1.09(12)	1.15(12)	1.18(12)	1.18(12)
47 Ag	9.18	13.32	---	7.77(10)	3.95(11)	7.63(11)	1.17(12)	1.43(12)	1.62(12)	1.67(12)	1.68(12)	---
56 Ba	6.90	12.11	1.26(10)	1.84(11)	6.51(11)	1.08(12)	1.49(12)	1.74(12)	1.90(12)	1.94(12)	1.93(12)	---
73 Ta	7.64	9.11	1.06(10)	3.07(11)	8.80(11)	1.32(12)	1.68(12)	1.90(12)	2.04(12)	2.07(12)	2.08(12)	---
74 W	6.20	9.02	3.12(10)	3.61(11)	1.00(12)	1.50(12)	1.92(12)	2.17(12)	2.33(12)	2.36(12)	2.36(12)	---
79 Au	8.07	8.55	9.49(9)	3.40(11)	9.08(11)	1.31(12)	1.64(12)	1.85(12)	1.99(12)	2.02(12)	2.02(12)	---
82 Pb	6.73	8.50	2.01(10)	4.09(11)	1.02(12)	1.43(12)	1.77(12)	1.97(12)	2.10(12)	2.14(12)	2.13(12)	---
92 U	(d)	7.64	1.06(11)	9.49(11)	1.95(12)	2.59(12)	3.05(12)	3.29(12)	3.45(12)	3.48(12)	3.46(12)	---

(a) In determining threshold energies, isotopes constituting less than 1% of the natural material are disregarded.
(b) Parameter ϵ_0 corresponds roughly to the critical energy. See text for explanation of values used.
(c) Integer in parentheses is the power of 10 by which to multiply.
(d) Effective threshold for photofission is 5.4 MeV (Di75); (γ, n) threshold is 6.13 MeV.

Table 2. Empirical parameters describing neutron yield very close to threshold.

Material	k_{th} (MeV)	Assuming Linear Rise from Threshold					Lorentz Resonance Cross Section				
		Y(1.0)[a] (neutrons per electron)	Slope[b] Assumed (mb/MeV)	Y_R(lin)[c]	N(lin)[d] (0.1 - 1.0)	N(lin)[d] (1.0 - 2.0)	Y(1.0)[a] (neutrons per electron)	$S(k_{th})$ (mb)	Y_R(res)[c]	N(res)[d] (0.1 - 1.0)	N(res)[d] (1.0 - 2.0)
^{12}C	18.72	2.63(-8)	0.706	0.155	3.47	3.53	(e)	---	---	---	---
^{27}Al	13.03	1.03(-8)	0.294	0.214	3.37	3.52	(e)	---	---	---	---
^{Nat}Fe	11.21	---	---	---	---	---	7.44(-7)	6.14	0.406	2.34	2.63
(f)^{Nat}Ni	11.38	8.46(-8)	(9.07)	(0.319)	(3.21)	(3.65)	(e)	---	---	---	---
^{58}Ni	12.19	1.18(-7)	4.41	0.316	3.21	3.44	(e)	---	---	---	---
^{60}Ni	11.38	2.62(-7)	9.07	0.318	3.21	3.44	8.10(-7)	7.09	0.420	2.32	2.63
(f)^{Nat}Cu	9.91	9.26(-8)	(9.02)	(0.328)	(3.20)	(3.77)	3.82(-7)	(9.40)	(0.432)	(2.31)	(3.03)
^{63}Cu	10.84	2.97(-7)	9.84	0.325	3.20	3.43	8.88(-7)	7.35	0.434	2.32	2.65
^{65}Cu	9.91	3.00(-7)	9.02	0.328	3.20	3.43	1.23(-6)	9.40	0.430	2.31	2.62
^{Nat}Ag	9.18	5.63(-7)	18.61	0.443	3.09	3.33	3.05(-6)	26.20	0.568	2.19	2.53
^{Nat}Ba	6.90	5.30(-7)	13.91	0.525	3.05	3.25	1.67(-6)	11.32	0.677	2.15	2.49
^{Nat}Ta	7.64	1.14(-6)	32.36	0.648	3.00	3.13	3.05(-6)	22.70	0.824	2.09	2.45
^{Nat}W	6.20	8.14(-7)	12.99	0.684	2.99	3.12	2.14(-6)	12.40	0.870	2.08	2.41
^{Nat}Au	8.07	1.97(-6)	60.42	0.682	2.99	3.11	5.53(-6)	45.27	0.851	2.07	2.41
(f)^{Nat}Pb	6.73	3.28(-7)	(34.27)	(0.818)	(3.03)	(3.87)	9.89(-7)	(23.33)	(1.21)	(2.19)	(3.26)
^{206}Pb	8.12	2.14(-6)	68.52	0.699	2.98	3.10	5.32(-6)	45.30	0.876	2.07	2.41
^{207}Pb	6.73	1.33(-6)	34.27	0.720	2.98	3.09	3.41(-6)	23.33	0.904	2.07	2.39
^{208}Pb	7.38	1.68(-6)	48.13	0.710	2.98	3.10	4.51(-6)	34.41	0.889	2.07	2.40
^{Nat}U	(g)	2.48(-6)	(53.95)	(0.829)	(2.97)	(3.23)	4.58(-6)	(21.36)	(1.29)	(2.13)	(2.52)

(a) Yield at $E_0 - k_{th} = 1.0$ MeV. Integer in parentheses is power of ten by which to multiply.

(b) Slope of photoneutron cross section from threshold k_{th} to $E_0 - k_{th} = 2$ MeV, assuming linear rise from zero.

(c) Reduced yield Y_R at $E_0 - k_{th} = 1.0$ MeV. See equations (8) and (11) of text for meaning of Y_R(lin) and Y_R(res), respectively.

(d) Exponent N for equation (9), averaged over indicated inverval: $E_0 - k_{th} = (0.1 - 1.0)$ or $(1.0 - 2.0)$ MeV.

(e) Lorentz resonance parameterization unsuitable or unavailable.

(f) Where the natural material is calculated by the explicit combination of separate isotopes having different thresholds (Ni, Cu, Pb), the parameters for the separate isotopes are also given. In these cases the values of Y_R and N for the natural material (in parentheses) are based on the slope or cross section assumed for the lowest threshold, and must be considered approximate.

(g) Differing thresholds for photofission (effectively 5.4 MeV) and (γ, n) processes (6.13 MeV) are disregarded and an intermediate effective threshold value of 6.00 MeV is used instead. Derived parameters (in parentheses) must be considered as approximate.

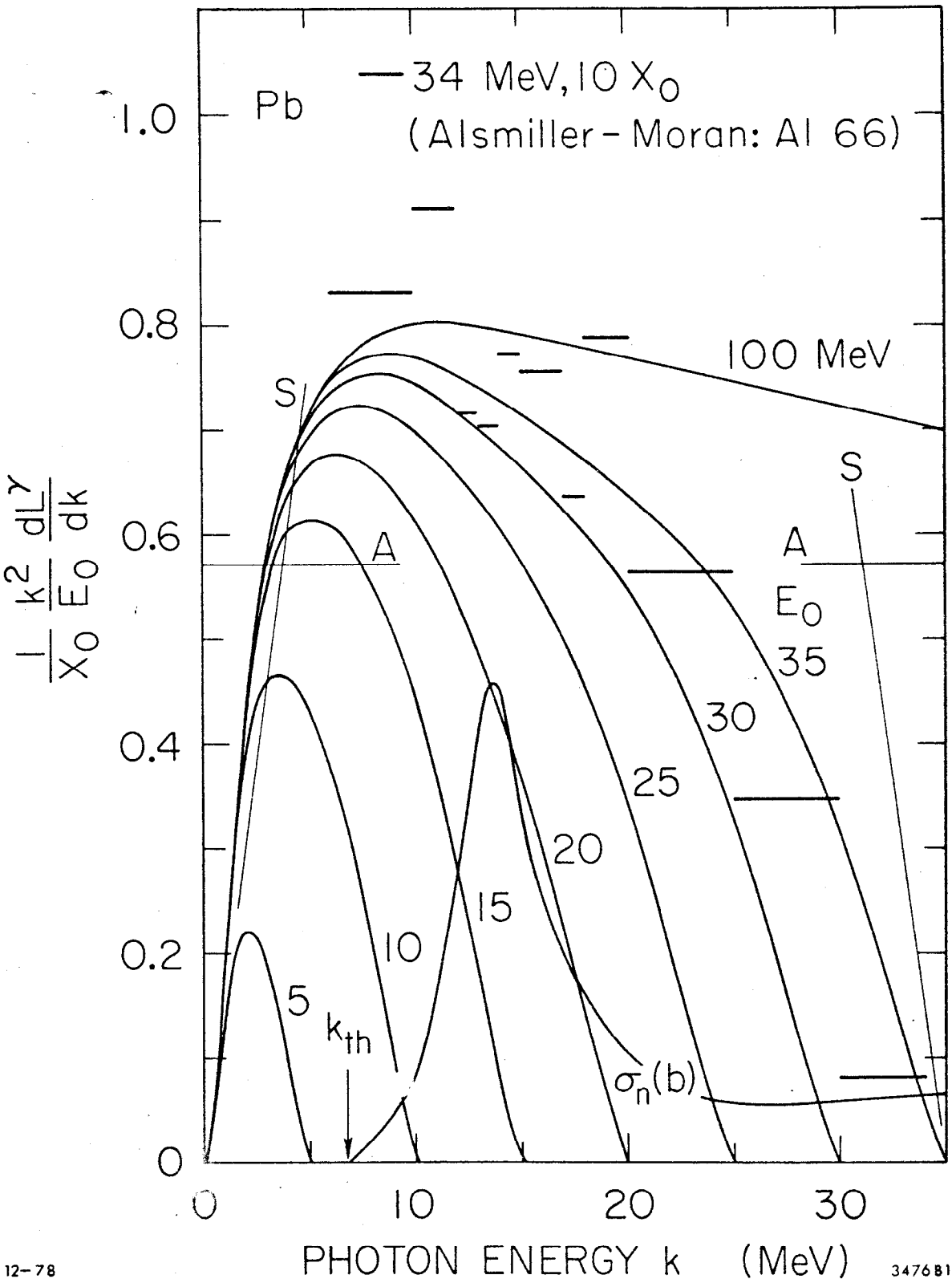
Pb
—34 MeV, 10 X_0
(Alsmiller-Moran: Al 66)
100 MeV
S
A
E_0
35
30
25
20
15
10
5
k_{th}
σ_n(b)
$\frac{1}{X_0}\frac{k^2}{E_0}\frac{dL^\gamma}{dk}$
1.0
0.8
0.6
0.4
0.2
0
0
10
20
30
PHOTON ENERGY k (MeV)
12-78
347681

Fig. 1

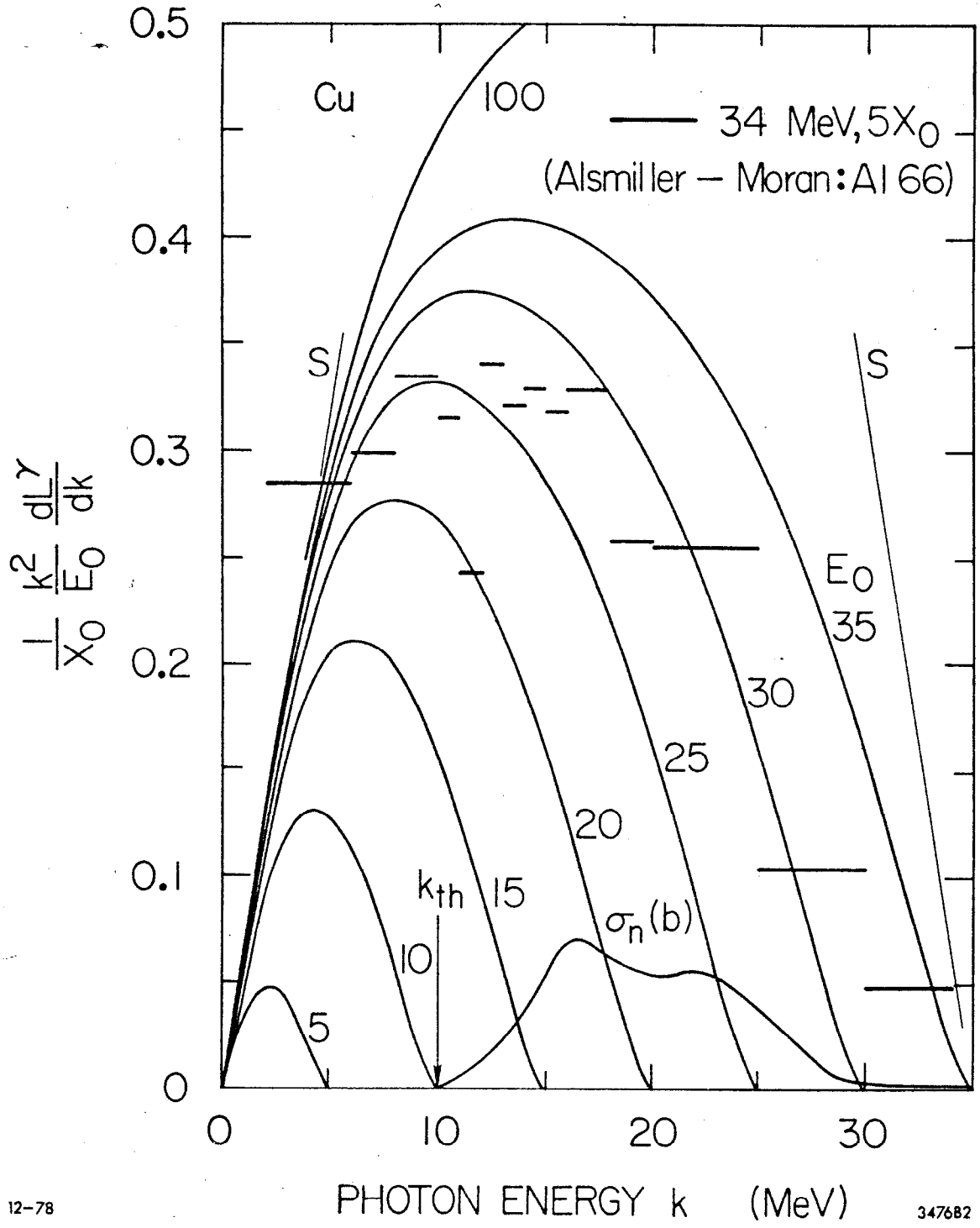
0.5
0.4
0.3
0.2
0.1
0
Cu
100
34 MeV, 5X0
(Alsmiller – Moran: Al 66)
S
S
E0
35
30
25
20
15
10
5
kth
σn (b)
0
10
20
30
PHOTON ENERGY k (MeV)
1/X0 k²/E0 dL^γ/dk
12-78
347682

Fig. 2

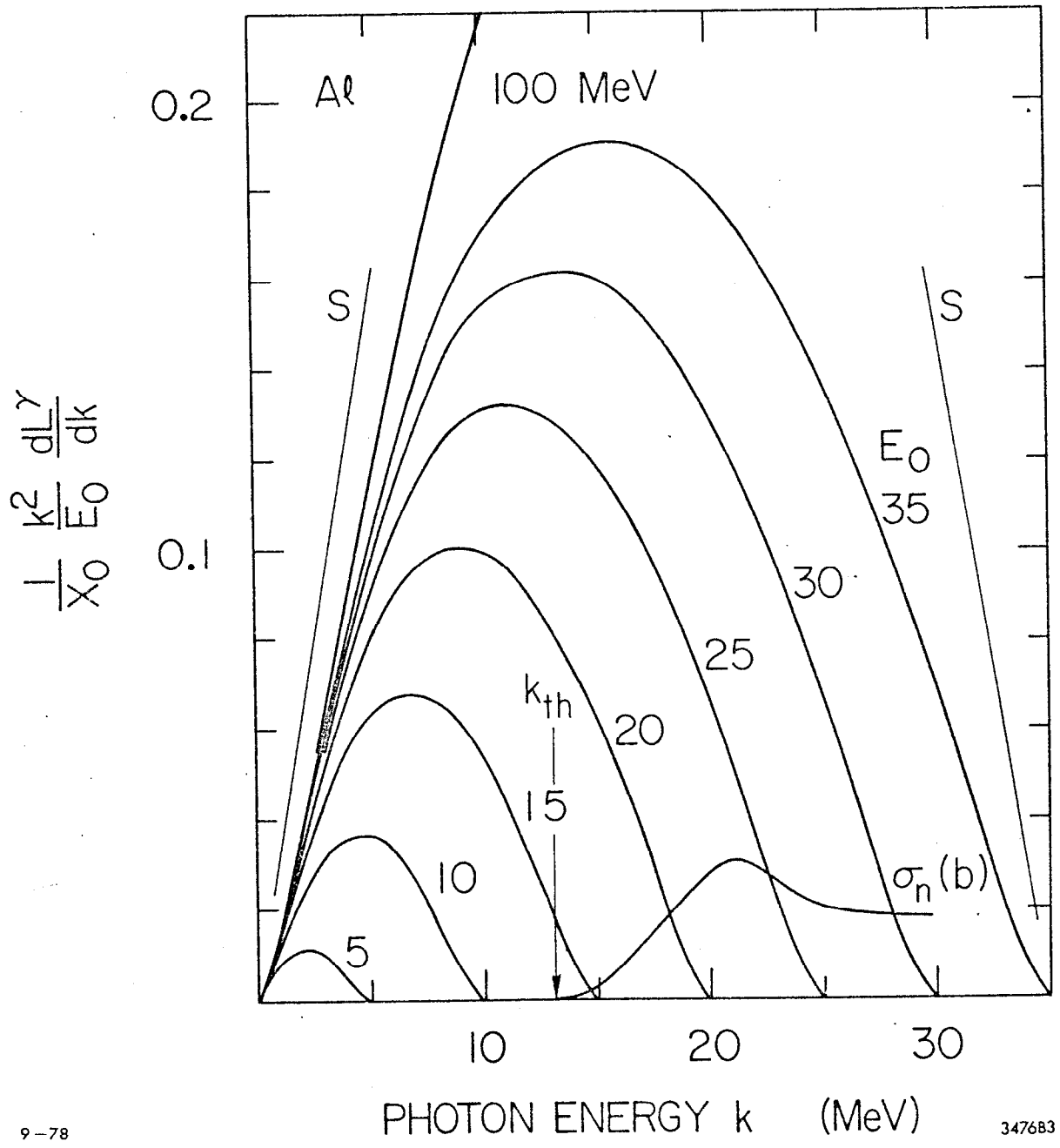
Al
100 MeV
0.2
0.1
S
S
E_0
35
30
25
20
15
10
5
k_{th}
σ_n(b)
10
20
30
$\frac{1}{X_0}\frac{k^2}{E_0}\frac{dL^\gamma}{dk}$
PHOTON ENERGY k (MeV)
9-78
347683

Fig. 3

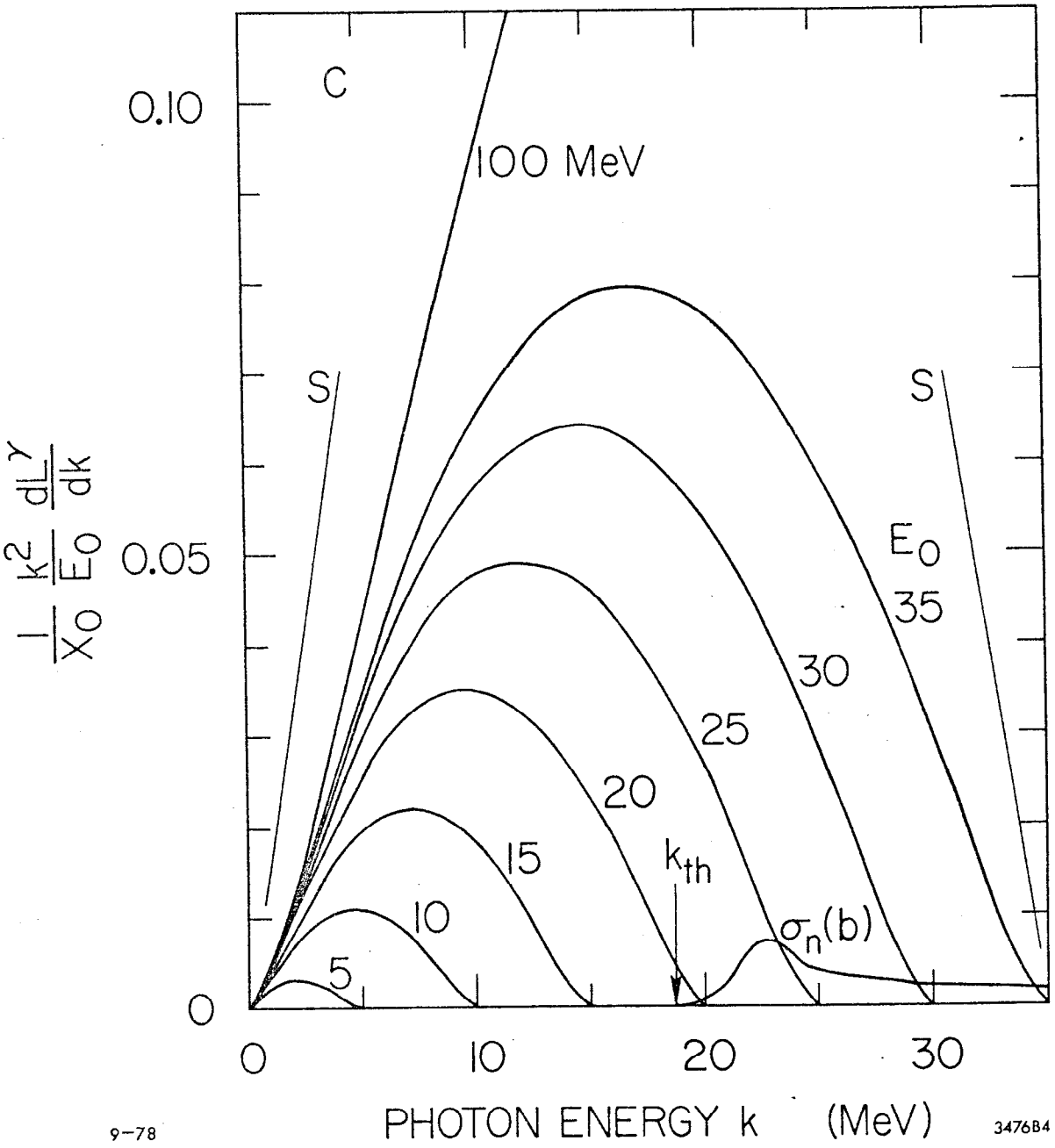
0.10
0.05
0
C
100 MeV
S
S
E_0
35
30
25
20
15
10
5
k_{th}
σ_n(b)
0
10
20
30
$\frac{1}{X_0}\frac{k^2}{E_0}\frac{dL^\gamma}{dk}$
PHOTON ENERGY k (MeV)
9-78
3476B4

Fig. 4

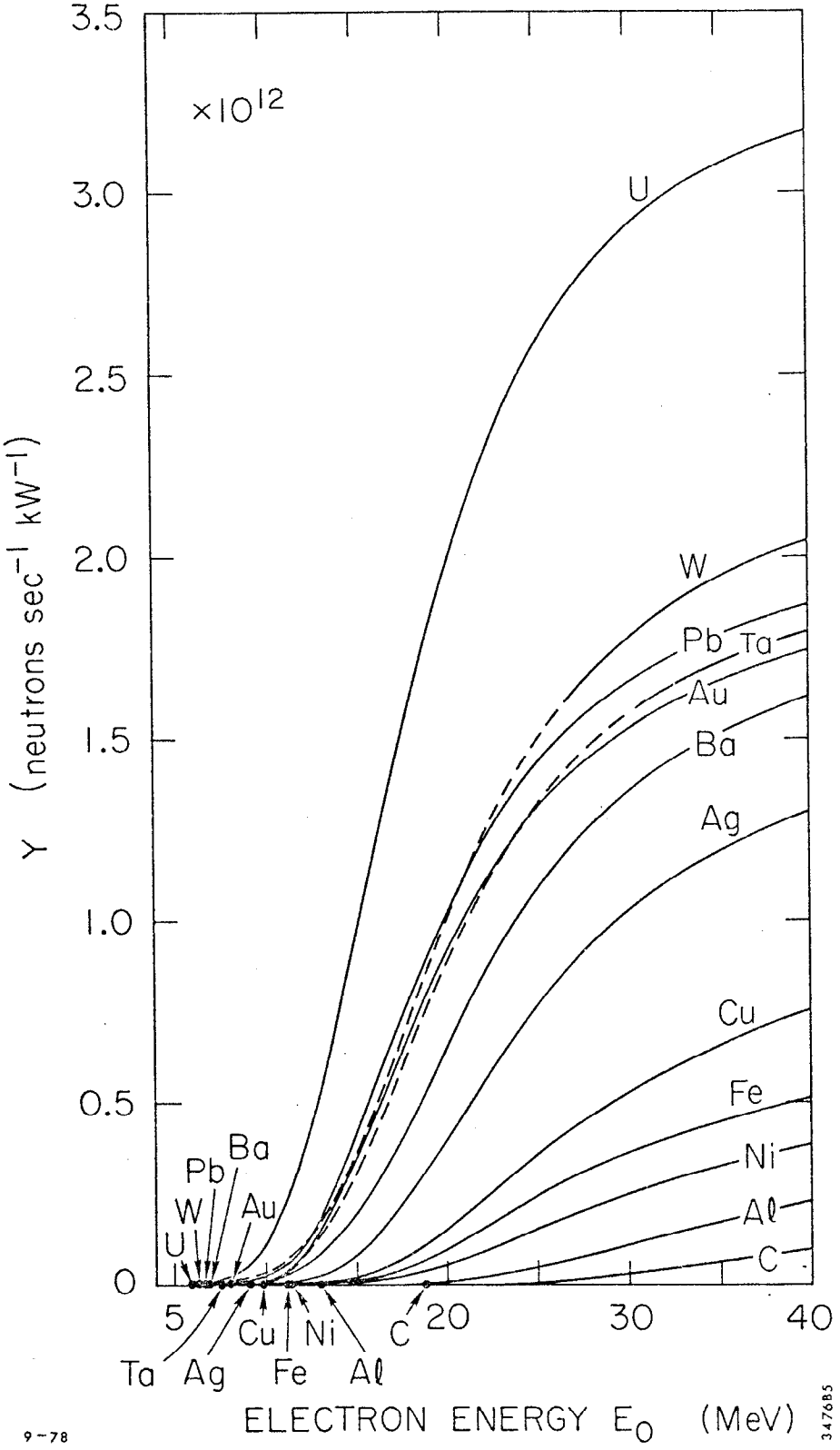
3.5
×10^12
3.0
2.5
2.0
1.5
1.0
0.5
0
Y (neutrons sec^-1 kW^-1)
U
W
Pb
Ta
Au
Ba
Ag
Cu
Fe
Ni
Al
C
5
20
30
40
Ta
Ag
Cu
Fe
Ni
Al
C
ELECTRON ENERGY E0 (MeV)
9-78
347685

Fig. 5

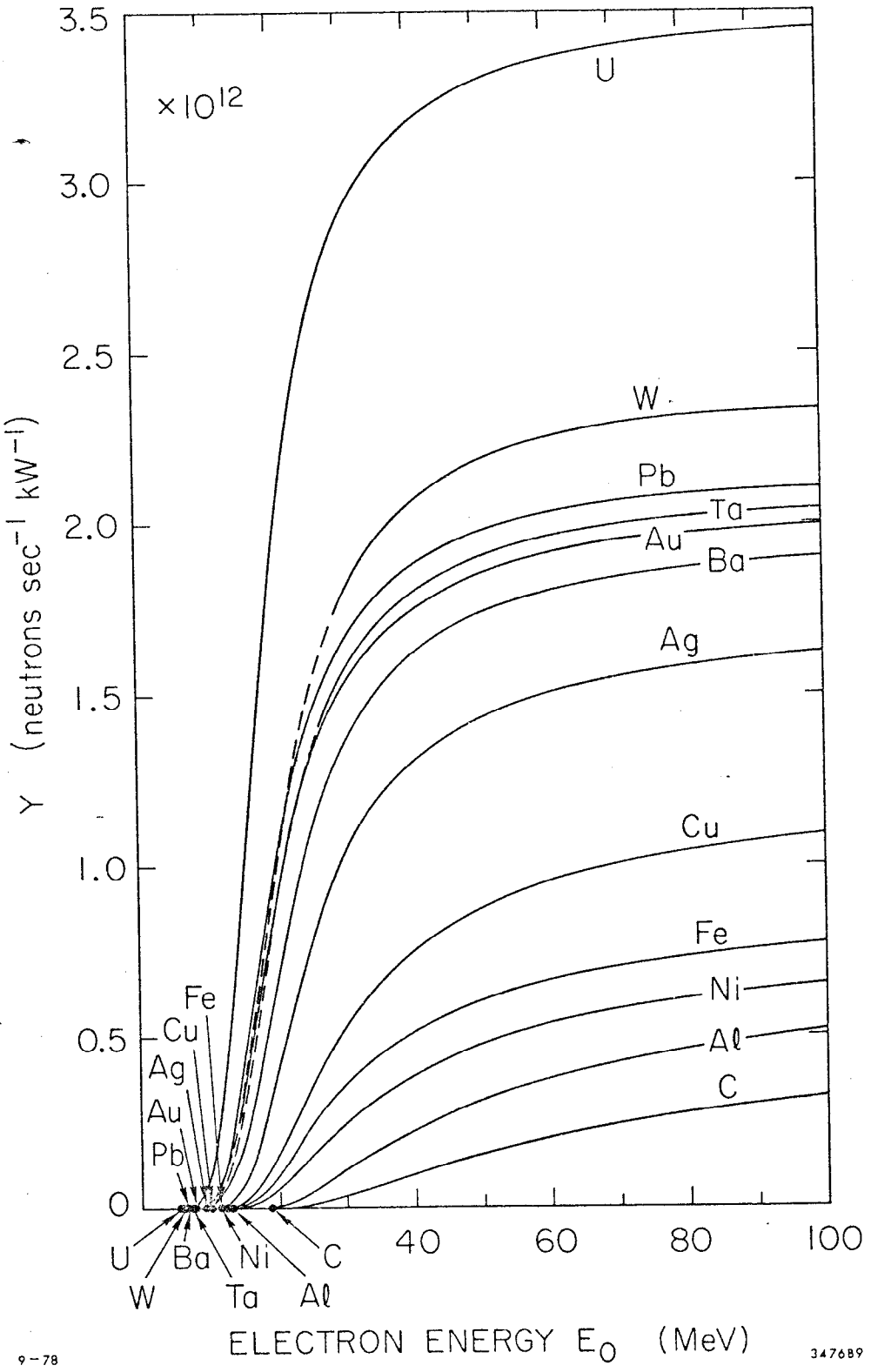
3.5
3.0
2.5
2.0
1.5
1.0
0.5
0
×10^12
Y (neutrons sec^-1 kW^-1)
U
W
Pb
Ta
Au
Ba
Ag
Cu
Fe
Ni
Al
C
Fe
Cu
Ag
Au
Pb
U
W
Ba
Ta
Ni
Al
C
40
60
80
100
ELECTRON ENERGY E0 (MeV)
9-78
347689

Fig. 6

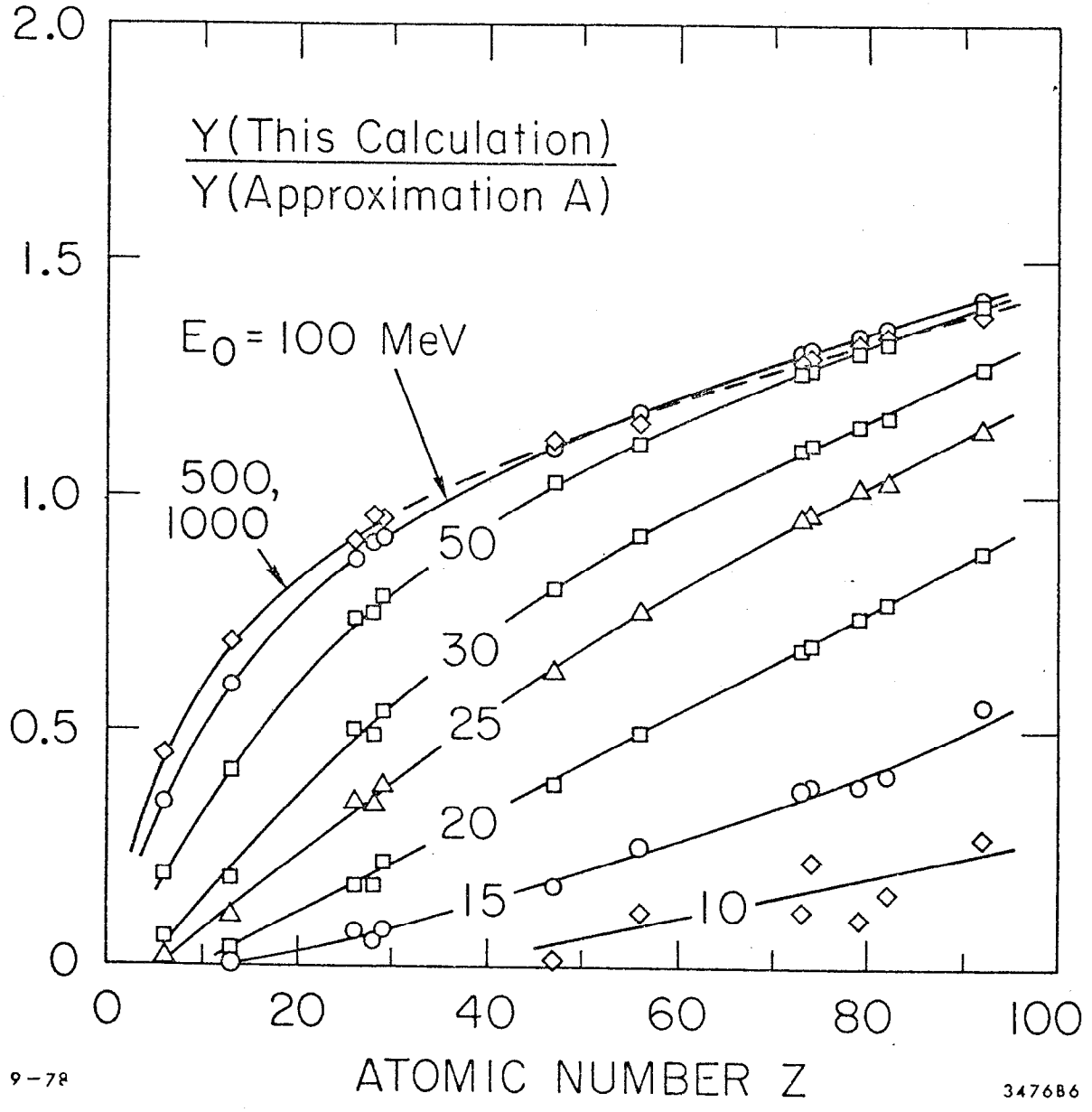
2.0
1.5
1.0
0.5
0
Y(This Calculation)
Y(Approximation A)
E_0 = 100 MeV
500,
1000
50
30
25
20
15
10
0
20
40
60
80
100
ATOMIC NUMBER Z
9-78
347686

Fig. 7

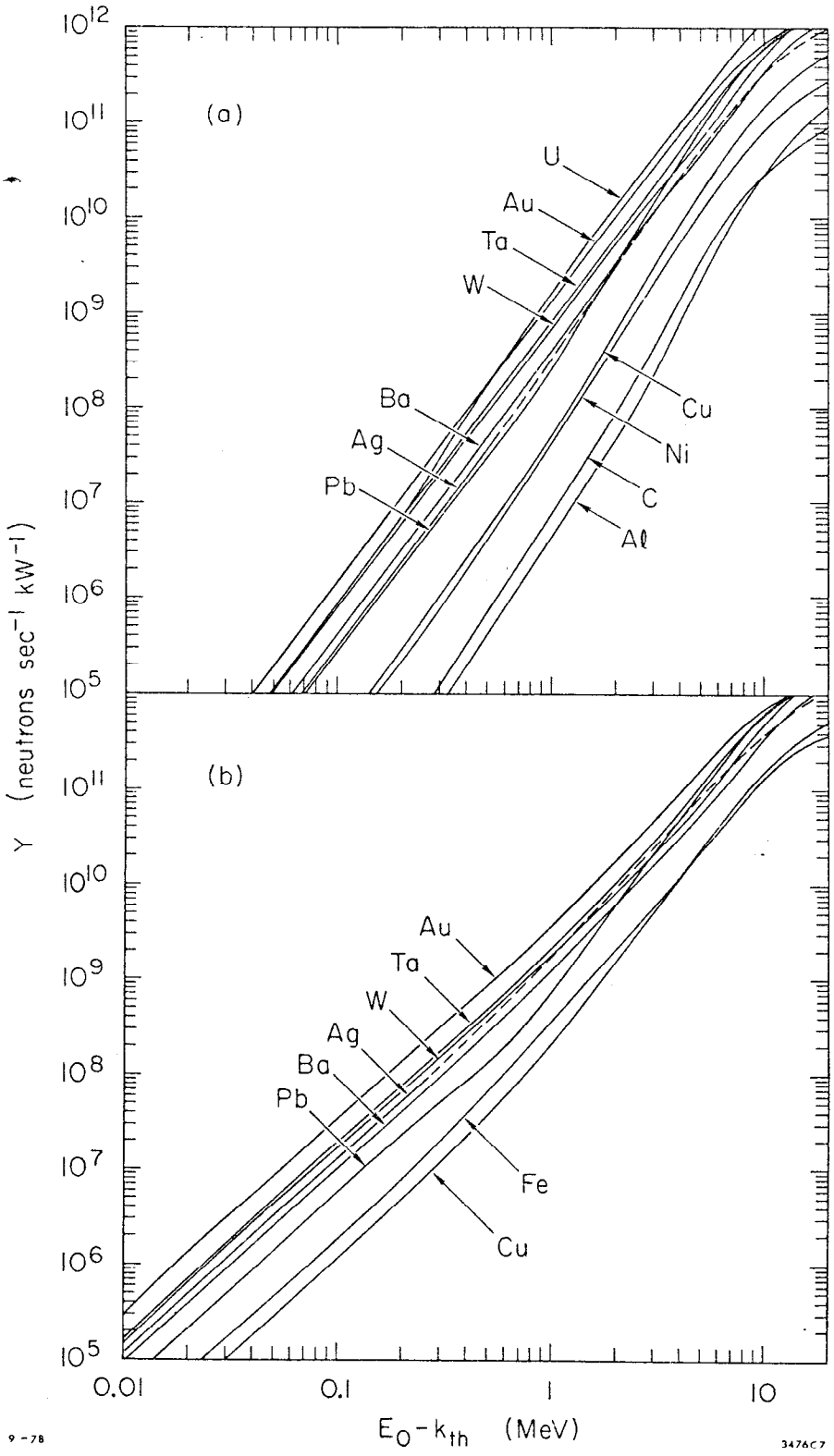
(a)
U
Au
Ta
W
Ba
Ag
Pb
Cu
Ni
C
Al
(b)
Au
Ta
W
Ag
Ba
Pb
Fe
Cu
Y (neutrons sec⁻¹ kW⁻¹)
10¹²
10¹¹
10¹⁰
10⁹
10⁸
10⁷
10⁶
10⁵
0.01
0.1
1
10
E₀ - k_th (MeV)
9-78
3476C7

Fig. 8

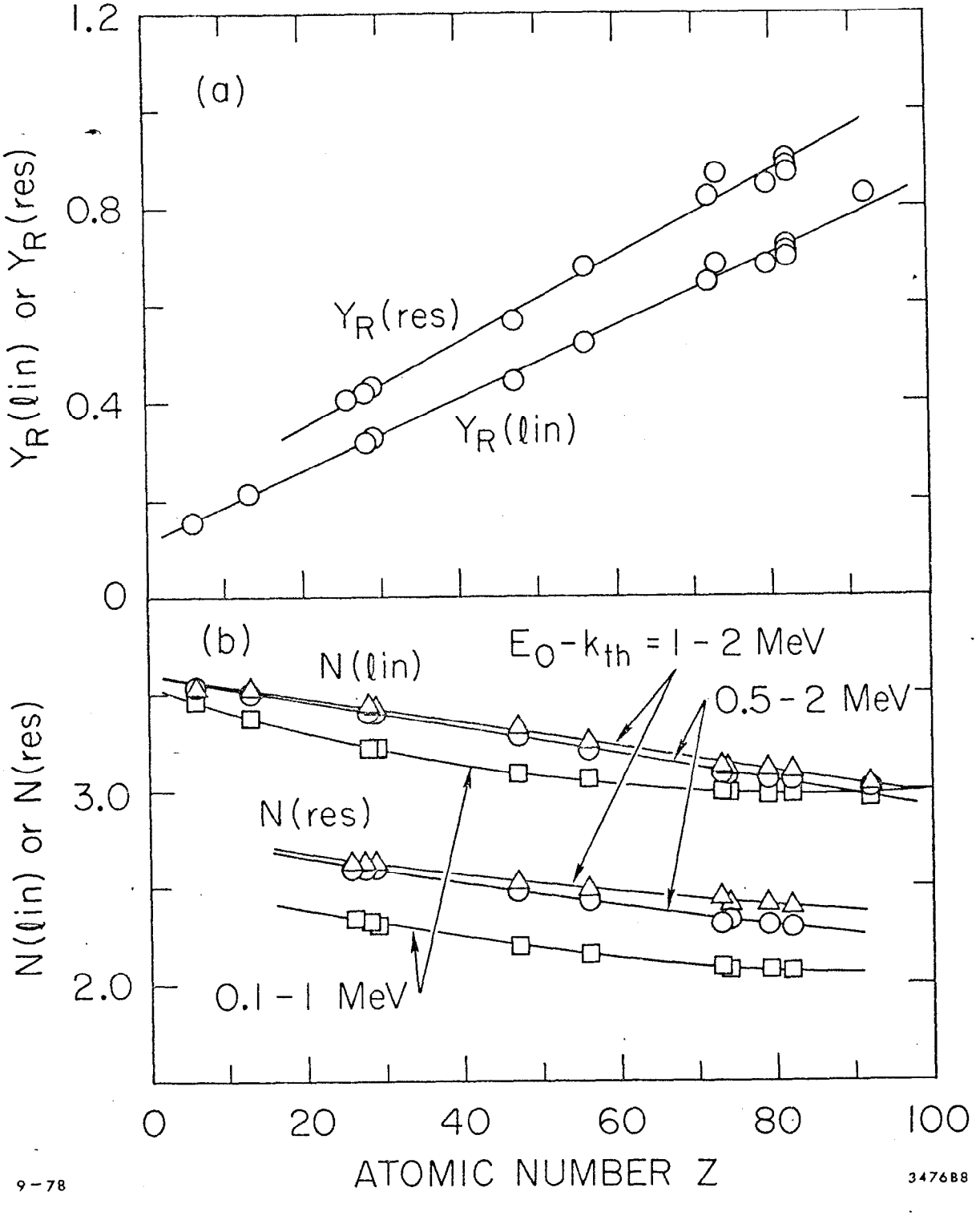
1.2
0.8
0.4
0
(a)
$Y_R(\ell in)$ or $Y_R(res)$
$Y_R(res)$
$Y_R(\ell in)$
(b)
N(ℓin)
$E_0 - k_{th}$ = 1 - 2 MeV
0.5 - 2 MeV
N(res)
0.1 - 1 MeV
N(ℓin) or N(res)
3.0
2.0
0
20
40
60
80
100
ATOMIC NUMBER Z
9-78
347688

Fig. 9